Chapter

Nanostructured Materials for the Development of Superhydrophobic Coatings

Jeyasubramanian Kadarkaraithangam, Thangaiyanadar Suyambulingam Gokul Raja, Silambuselvan Parani Bramma Nayagi and Karthikeyan Krishnamoorthy

Abstract

This chapter describes the results of developing superhydrophobic coatings using porous ZnO nanostructures impregnated metal stearates and their applications. The porous ZnO nanostructures with a surface area of 9.7 m^2/g and pores in the range from 200 to 400 nm have been prepared via precipitation cum calcination route. The superhydrophobic coatings comprising ZnO/metal stearate film have been deposited using a spray coating method. The developed superhydrophobic films possess a water contact angle of 161° that can be explained using the Cassie-Baxter model. The prepared films exhibited excellent floating properties and high load-bearing characteristics over a prolonged time. Additionally, the self-cleaning properties of the developed superhydrophobic films towards dust removal and self-cleaning urinary coatings are also demonstrated. This chapter collectively presented the novel applications of superhydrophobic coating in the development of biomedical coatings and applications in water surveillance and underwater robotics.

Keywords: nanomaterials, superhydrophobic, Cassie-Baxter equation, functional coatings, nanoscale roughness

1. Introduction

Superhydrophobic surfaces received many research interest from academic to industrial sectors due to their intriguing self-cleaning properties [1–4]. The study on superhydrophobic surfaces was initiated during early 1907 when Ollivier observed a contact angle of ~180° for surfaces modified with soot, lycopodium powder, and arsenic trioxide [1]. Later, Coghill and Anderson (in 1923) studied the surface modification of galena via deposition of stearic acids leading to achieve a water contact angle (WCA) of 160° [1]. Until the 1990s, minimal research work has been carried out on superhydrophobic surfaces. In contrast, it was reactivated in 1997 when Neinhuis and Barthlott discussed the origin of superhydrophobicity via the principle of "lotus effect" [5]. Many researchers have focused on superhydrophobic surfaces by mimicking nature and fabricating similar structures via artificial methods through

surface modification. Besides fundamental understanding of the superhydrophobic phenomenon, researchers currently focuses on extending the application of superhydrophobic surfaces like self-cleaning coatings, friction reduction coatings on ship hulls, corrosion prevention oil–water separation, and antibacterial textiles/bandages [6–9]. Generally, roughness plays a vital role in the hydrophobicity of a hydrophobic solid. Flat solids display almost 100° to 120° contact angles for water and reach up to 160° to 175° if they are rough or micro/nanotextured. Such improved superhydrophobic behavior is not only due to the solids' surface chemistry alone [10]. There are two distinct processes involved in the enhancement of superhydrophobic properties that can be explained based on the (i) Wenzel model and (ii) Cassie-Baxter model [11, 12]. The Wenzel model relies on the surface roughness induced high surface area of the solid resulting in superhydrophobic nature. The Cassie model revealed that the air trapped below the drop could also result in stable superhydrophobic properties. In both models, an apparent contact angle θ^* of a drop on the surface of a rough substrate/solid will be formed via reducing the surface energy of a drop to Young's contact angle θ (determined on a flat surface of the same) [10].

Naturally, the water repellent properties (superhydrophobic surfaces) can be seen in many plant surfaces (lotus leaves), and animal furs, so on [13]. For instance, lotus leaves are considered as one of the finest examples of superhydrophobic surfaces. The WCA of the lotus leaf is about ~162° with a hysteresis of 2°. Barthlott and Neihuis study the micro-structure of lotus leaf using a scanning electron microscope (SEM) [14]. They demonstrated the presence of two different ranges of roughness present in lotus leaf viz. (i) one with 10 μm (rough structure) and (ii) other with 100 nm (fine structure). These studies confirmed micro- and nano-textured surfaces on the lotus leaf that lead to the origin of their self-cleaning properties [15]. To date, there are different methods used for the creation of superhydrophobic surfaces that can be broadly classified as (i) Top-down and (ii) bottom-up methods. Top-down approaches include the costly lithographic process, template-assisted fabrication methods, and delicate surfaces' plasma treatment [16–18]. Bottom-up approaches include self-assembled layers/films, chemical deposition, and layer-by-layer (LBL) deposition, etc., [19–21]. The available methods from the bottom-up approaches are considered cost-effective and scalable compared to the top-down methods. More importantly, synergistic methods involving both top-down and bottom-up methods are also in practice. Most of them rely on solution casting, phase separation, electrospinning/spraying, and nanostructure impregnated polymer composite films [22, 23]. The superhydrophobic surfaces/coatings possess numerous applications in automobile windows, optical windows for electronic devices, eyeglasses, fluidic drag reduction, enhanced water supporting force, water corrosion prevention, and humidity proof coatings, antibiofouling, self-cleaning textiles, and oil–water separation, etc. [24–27]. Additionally, the superhydrophobic materials as electrodes for batteries and fuel cells result in their extended shelf-life time as experimentally demonstrated by Lifton et al. [28]. Recently, studies demonstrated that the superhydrophobic coatings could also be used for applications such as anti-icing, anti-fogging, and anti-frosting sectors.

The role of nanostructured materials in superhydrophobic coatings is rapidly rising mainly due to their exceptional physical/chemical properties [29]. The choice of nanostructures over their bulk counterparts for superhydrophobic coatings is due to the increased surface area and high roughness on the surfaces. The nanostructured materials are mostly used as fillers in polymers to modify their surface roughness and porosity of the polymer surfaces, leading to superhydrophobic properties. Additionally, the choice of nanomaterials in superhydrophobic coatings also enhanced their durability and focused on biomedical applications such as creating antibacterial textiles, medical implants, etc. [29–31]. This chapter discusses the recent trends in the development of nanostructured materials based on superhydrophobic coatings and their applications.

2. Methods

2.1 Preparation of porous ZnO nanostructures

A facile precipitation cum calcination route was used for the preparation of porous ZnO nanoparticles [32]. Briefly, appropriate amount of zinc nitrate (4 g) was dissolved in distilled water, followed by the addition of polyethylene glycol (PEG) (3 g) and hexamine (3 g). The entire precursor solution is subjected to a vigorous stirring process using a magnetic stirrer for 30 minutes at a temperature of 60 °C. Following this, the ammonia solution was added to the precursor solution until their pH reached 9. After that, the solution is allowed to gelation process by placing them in a hot plate at the temperature of 90 °C, which results in the formation of a dark brown gel. After 4 hours, the dried brownish gel was placed in a silica crucible and calcined at a temperature of 500 °C for 2 h that finally lead to the formation of white-colored porous ZnO nanostructures.

2.2 Synthesis of copper stearate and magnesium stearate

The metal (copper/magnesium stearate powders) were prepared via a precipitation method using metal salts, stearic acid, and ammonia, as reported in our recent works [32, 33].

2.3 Fabrication of superhydrophobic films via spray coating process

A spray coating process is used to fabricate the superhydrophobic films comprising ZnO/metal stearate with the various weight ratio of ZnO in our recent study [32]. The coating thickness was varied by spraying the solution from different time intervals ranging from 30 seconds to 30 minutes.

3. Results and discussion

3.1 Characterization of porous ZnO nanostructures

Figure 1(A) shows the X-ray diffraction (XRD) pattern of ZnO nanostructures prepared via the calcination route explained in section 2.1. High intense sharp diffraction peaks are seen in **Figure 1(A)** matched with the wurtzite structure of ZnO ((JCPDS No. 89–7102) [34]. The Raman spectrum of the prepared ZnO nanostructures (given in **Figure 1(B)**) indicated a sharp band located at 437 cm^{-1} as a result of E_2 (high) mode vibrations [35]. **Figure 1(C, D)** represents the deconvoluted X-ray photoelectron spectroscopy of Zn and O states present in the ZnO nanostructures. The Zn 2p states (given in **Figure 1(C)**) showed the presence of two peaks corresponding to the Zn $2p_{3/2}$ (at 1022 eV) and Zn $2p_{1/2}$ (at 1045 eV), respectively. A value of 23 eV is obtained for the difference between the peak positions of Zn $2p_{3/2,}$ and Zn $2p_{1/2}$ states that matched with the reported ones and indicates that Zn possesses an oxidation state of +2 in the synthesized ZnO nanostructures [32]. The O 1 s spectrum evidences the broad peak centered at 532 eV (given in **Figure 1(D)**) arises from the oxygen content present in the wurtzite ZnO [35]. The field emission scanning electron micrographs (FE-SEM) of the as prepared ZnO nanostructures (given in **Figure 1(E)** and **(F)**) showed the presence of nanoparticles with a high amount of pores. The high magnification micrograph (**Figure 1(F)**) evidences the honeycomb-like porous ZnO nanostructures with pore sizes ranging from 200 to

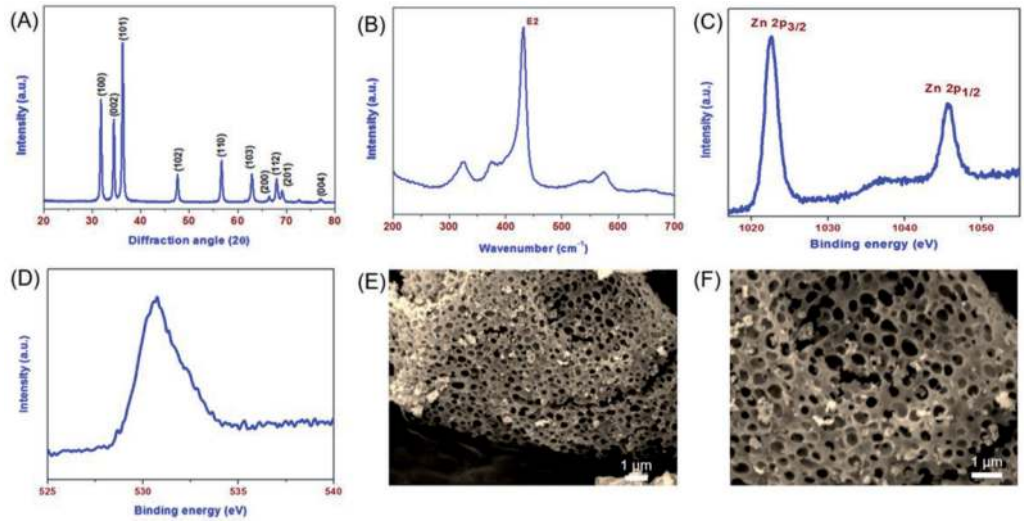

Figure 1.
(A) X-ray diffraction pattern, (B) laser Raman spectrum, (C) Zn 2p core-level X-ray photoelectron spectrum, and (D) O 1 score-level photoelectron spectrum of porous ZnO nanostructures and scanning electron micrographs of porous ZnO nanoparticles with (E) low and (F) high magnification.

400 nm. The Brunauer-Emmet-Teller (BET) analysis using the Barrett–Joyner–Halenda (BJH) method of the ZnO nanostructures revealed the Type IV isotherm with a hysteresis (data not shown) highlighting the presence of mesoporous nature [36]. The prepared ZnO nanostructures possess a pore volume and surface area of about 0.028 cm^3/g, and 9.7 m^2/g. The obtained high surface area of the ZnO nanostructures is due to the role of PEG in the preparation. The guest-host chemistry of metal ions with polymer matrix (i.e., Zn^{2+} ions as a guest in the PEG host matrix) results in the formation of mesoporous ZnO nanostructures via decomposition of PEG during the calcination process.

3.2 Characterization of copper stearate

The formation of copper stearate via precipitation method was studied using Fourier transformed infra-red spectroscopy (FT-IR) and XRD analysis (given in **Figure 2(A,B)**). During the formation of copper stearate from stearic acid using copper salts, the carboxyl group's and hydrogen atom in the stearic acid is replaced with the Cu ions. **Figure 2(A)** compares the FT-IR spectra of copper stearate to that of stearic acid. The presence of vibration due to the COO- group in stearic acid is noticed via its characteristic peak at 1700 cm^{-1} and is disappeared/shifted towards a lower peak position at 1583 cm^{-1}, respectively [37]. The sharp bands observed at 3352 (-OH) and 1046 cm^{-1} (C-O stretching) in the spectrum of stearic acid were disappeared in the FT-IR spectrum of copper stearate. Additionally, the FT-IR spectrum of copper stearate revealed the presence of characteristic bands at 2847, 2917, 1441, 720, and 880 cm^{-1} raised from the CH_2, C-H, C-C, CH_2 (rocking), and CH_3 rocking vibrations, respectively [38, 39]. The presence of characteristic diffraction peaks from 5° to 20° in the XRD pattern (given in **Figure 2(B)**) confirmed the formation of copper stearate [32, 38].

3.3 Characterization of ZnO/copper stearate composite films

Figure 2(C) shows the FT-IR spectrum of bare ZnO nanostructures and ZnO/copper stearate composite films. The presence of vibration bands centered at 518 and

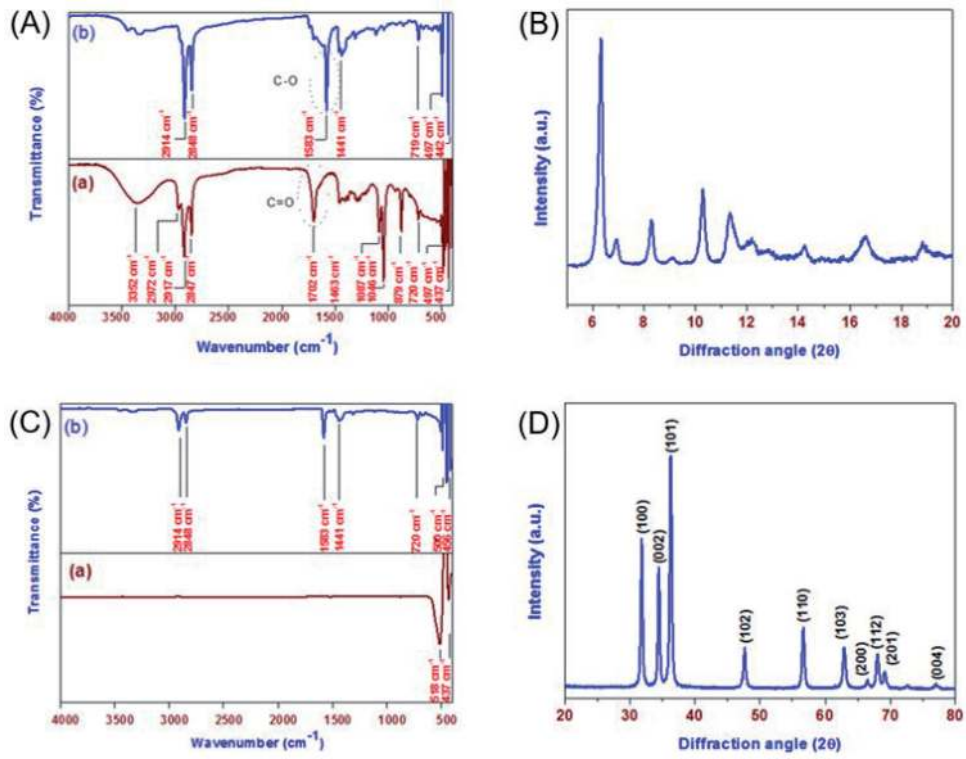

Figure 2.
(A) Fourier transform infrared spectrum and (B) X-ray diffraction pattern of copper stearate, (C) FT-IR spectrum of porous ZnO and ZnO/copper stearate coatings, (D) X-ray diffraction pattern of ZnO/copper stearate coatings.

437 cm^{-1} was raised from the Zn-O vibrations present in ZnO nanostructures [40]. The FT-IR spectrum of ZnO/copper stearate film given in **Figure 2(C)** shows almost all the characteristics vibration bands of ZnO nanostructures and copper stearate with slight variation in their peak positions, that is due to the interaction between the ZnO nanostructures and copper stearate via guest-host chemistry. **Figure 2(D)** shows the XRD pattern of the ZnO/copper stearate coatings. The peaks corresponding to the crystalline ZnO nanostructures were visible in the XRD pattern, whereas the peaks due to the copper stearate were diminished/not observed. This is due to the low crystallinity of copper stearate compared to ZnO nanostructures' highly crystalline nature. **Figure 3(A)** depicts the SEM image of spray-coated ZnO/copper stearate films. It is quite challenging to distinguish ZnO nanostructures in the spray-coated films due to the low weight percentage of ZnO to that of copper stearate and better dispersibility of ZnO nanostructures in the copper stearate due to the ultrasonication process. The size of the pores present in the ZnO/copper stearate coatings was found to be in the range from 100 to 300 nm determined using ImageJ software [41]. Here, it is noteworthy that micron-sized ZnO in similar coatings resulted in irregular surface formation due to the low dispersion index of micron-sized ZnO. **Figure 3(B-D)** shows the elemental maps of Zn, O, and Cu components present in the ZnO/copper stearate coatings. The Zn map of the spray-coated films (shown in **Figure 3(B)**) indicated the presence of well-dispersed ZnO nanostructures in the copper stearate matrix. **Figure 3(C)** presents the oxygen map indicating the existence of array-like arrangement due to the chain-like structures of copper stearate in addition to the ZnO components of the coating. The mapping of copper elements in the spray coated films (given in **Figure 3(D)**) shows that the copper elements are randomly distributed in the films. Since the copper elements are attached

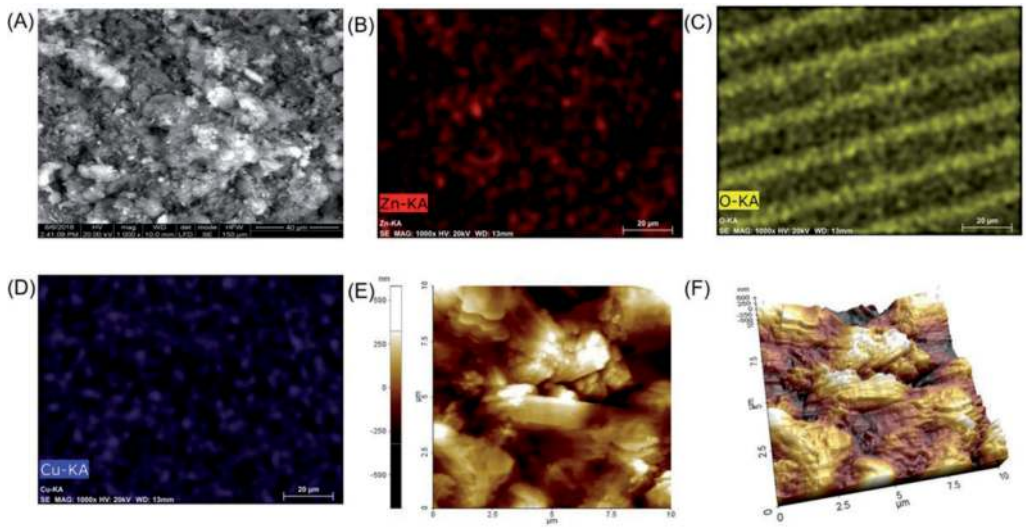

Figure 3.
Field emission scanning electron micrograph of (A) ZnO/copper stearate and (B-D) shows the elemental maps of Zn, O, and Cu present in these coatings and (E-F) 2D and 3D Atomic force micrograph of ZnO/copper stearate coatings.

to the end of the chain-like structure of copper stearate. More probably, the copper ends were attached to the glass substrates due to their hydrophilic nature leaving the hydrophobic methyl group on the exterior surfaces. The 2D and 3D topographic analysis of the spray coated ZnO/copper stearate films analyzed by atomic force micrograph is shown in **Figure 3(E, F)**. These studies demonstrated the existence of porous and rough surfaces nature of the spray-coated ZnO/copper stearate films.

3.4 Superhydrophobic properties of ZnO/copper stearate coatings

The water contact angle measurement was carried out for determining the superhydrophobic properties of the ZnO/copper stearate coatings with various loading ratios of ZnO nanostructures in the copper stearate matrix. The plain glass substrates possess a WCA of 27.4°, indicating their hydrophilic surfaces [42]. The bare copper stearate coatings (with low surface energy) on glass substrates possess a WCA of 152.4°, demonstrating their hydrophobic properties. It is expected that the inclusion of porous ZnO nanostructures in the copper stearate matrix might alter their roughness and thus improves the hydrophobicity. The effect of porous ZnO nanostructures loading ratio on the water repellent properties of the ZnO/copper stearate coatings is summarized in **Figure 4(A)**. It displayed that the superhydrophobic effect was not obtained in the composite films with a loading ratio of ZnO nanostructures until 0.01 g. The ZnO/copper stearate coatings displayed the superhydrophobic properties with a WCA of 161° when the ZnO weight percentage is increased up to 0.14 g. This can be due to the improvements in the films' roughness by the inclusion of highly-porous ZnO nanostructures. The mechanism of superhydrophobic effect achieved in the spray-coated films can be described via the Cassie-Baxter model using the following relation [43]:

$$\cos\theta^{*} = \varphi_s \cos\theta + \varphi_s - 1 \ldots \quad (1)$$

Here θ^{*}, φ_s and θ represents the apparent contact angle, substantial fraction in contact with liquid, and Young's contact angle, respectively. The substantial fraction of the bare copper stearate coating is about 0.197, and these values decrease with

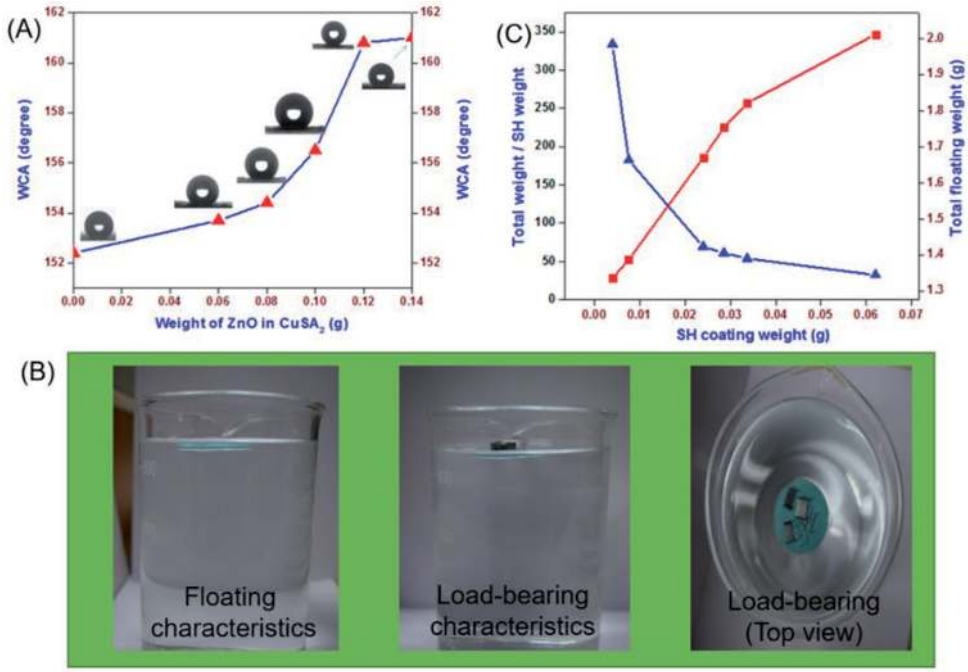

Figure 4.
(A) Water contact angle, (B) floating characteristics, and (C) load-bearing properties of ZnO/copper stearate coatings.

an increase in the loading ratio of porous ZnO. A low substantial fraction of about 0.094 was reached for the ZnO/copper stearate coatings with a ZnO loading of about 0.14 g. The observed decrease in solid fraction values indicated the enhancement in the surface roughness due to porous ZnO nanostructures' impregnation. A similar effect is not observed in films coated using non-porous ZnO or micron-sized ZnO powders. This further substantiates porous ZnO nanostructures' significance for modulating the roughness of copper stearate films to obtain superhydrophobic properties.

3.5 Floating and load-bearing characteristics of superhydrophobic ZnO/copper stearate coatings

Floating and load-bearing characteristics are major applications where superhydrophobic coatings for underwater robotics, monitoring water pollution, water quality analysis, and surveillance applications can be developed [44–46]. Based on the Archimedes principle, it is well known that any object (with density higher than water) will sink in water. However, water strider possesses the ability to float in water and stride freely on the water surface due to the hierarchical fibrous architecture of strider leg exhibiting superhydrophobic effect. The bare glass substrates immediately drown after placing in water solution, which can be explained using the Archimedes principle [47]. It is expected that superhydrophobic coatings can possess a floating nature. The floating characteristics of the spray-coated ZnO/copper stearate coatings (laid down) in the water solution is shown in **Figure 4(B)**. The fundamental mechanism of an object's floating nature will be achieved if the buoyancy force exerted by the object is higher than the drown force acts on it. The ZnO/copper stearate coatings on glass substrates float on water solution for more than a week without any noticeable sinking effects. Here, in addition to the buoyancy force, a curvature force acts on the surface of superhydrophobic coatings, acting against the drown force that enables them to float over a prolonged time. The superhydrophobic ZnO/

copper stearate coatings possess a trapped air film on their exterior surfaces leading to an excessive displaced volume of water. The entire phenomenon can be termed as super-buoyancy [48]. These studies demonstrated the plastron effect's vital role in the ZnO/copper stearate coatings' floating properties. The ZnO/copper stearate coatings' load-bearing characteristics are investigated by loading known mass (stapler pins) on their top surface during floating, as shown in **Figure 4(B)**. It showed that after loading a few stapler pins, there are no signs of sinking for the ZnO/copper stearate coatings. The effect of thickness of superhydrophobic ZnO/copper stearate coatings via different deposition times (180 to 1800 seconds) on their load-bearing properties is provided in **Figure 4(C)**. It showed that ZnO/copper stearate coatings with a high thickness (weight of about 0.062 g) remain floating and can bear about 0.3667 g (19 stapler pins) without sinking issues. **Figure 4(C)** illustrated that the ratio of net floating weight to the weight of ZnO/copper stearate coating decreases with increasing thickness. This can be explained based on the more inert/dead layers present in the coatings with high thickness. On the other hand, the capability of load-bearing is superior for thin coatings (deposition at 30 seconds) that can bear 52 pins (~333 times higher than their net weight). The findings on the floating and load-bearing characteristics of the superhydrophobic ZnO/copper stearate coatings can be applied for water floating micro-robots and surveillance applications.

3.6 Applications of superhydrophobic coatings towards self-cleaning urinary coatings

The superhydrophobic coatings' self-cleaning properties can be used for developing water-free urinaries, which doesn't require any systematic cleaning process to mollify unpleasant odor [49, 50]. Since the surface tension of water (71.2 mN/m) and urine (70 mN/m) are of similar values, it is expected that a water-repellent surface possesses a tendency to repel urine as well [51, 52]. The ZnO/magnesium stearate coatings showed excellent dye and urine-repellant properties, as shown in **Figure 5(a, b)**. It is observed that the droplets of urine samples roll off over the surface of ZnO/magnesium stearate coatings due to their extreme repellent

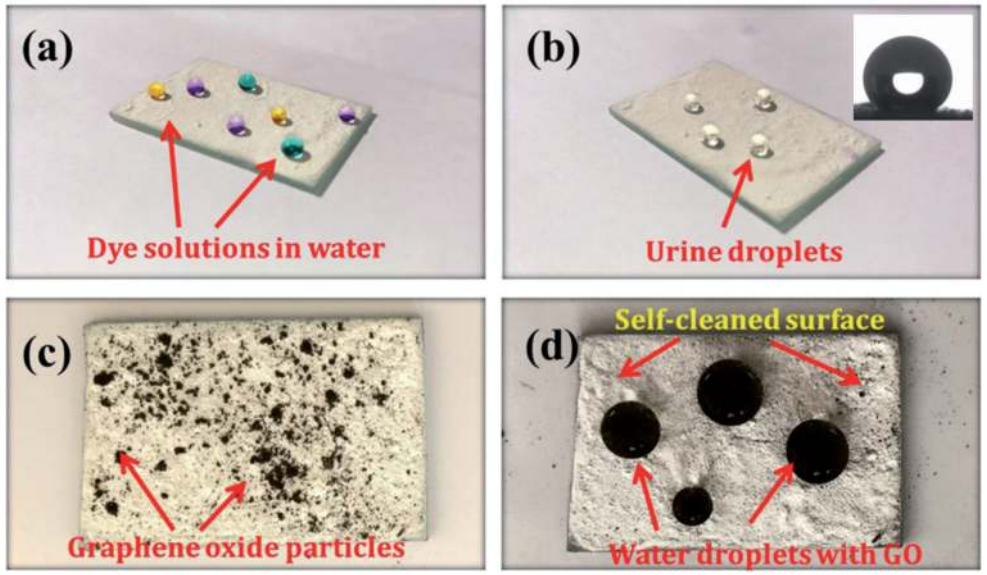

Figure 5.
Superhydrophobic applications of ZnO/magnesium stearate (a) dye repellency, (b) urine repellency, (c) spreading of graphene oxide (GO) dust on coatings, the (d) self-cleaning ability of ZnO/magnesium stearate to remove the GO dust.

properties [33]. The FT-IR spectrum measured after urine droplet tests on the ZnO/magnesium stearate showed the absence of vibration bands due to urine, which showed their excellent superhydrophobic effects [33]. Additionally, these superhydrophobic films' self-cleaning properties are also examined using graphene oxide as a dust spread on their surfaces. After adding few water droplets on their surface, the water droplets cleaned all the dust (graphene oxide) on their surfaces, as shown in **Figure 5(c, d)**, and ensures their self-cleaning properties.

4. Conclusions

In conclusion, the significant role of porous nanostructures for developing superhydrophobic coatings is demonstrated in this chapter. A cost-effective sonochemical approach combined with a spray coating process for the fabrication of superhydrophobic coatings is presented. The impact of nanostructures on the coatings' porosity is explained with the experimental findings like AFM micrograph and water contact angle measurements. The exciting applications of superhydrophobic coatings like water-floating properties, load-bearing applications, dust removal, self-cleaning urinary coatings are illustrated in this chapter.

Acknowledgements

The authors thank the Management and the Principal, Mepco Schlenk Engineering College, Sivakasi, for the constant encouragement and support.

Conflict of interest

"The authors declare no conflict of interest."

Author details

Jeyasubramanian Kadarkaraithangam[1*],
Thangaiyanadar Suyambulingam Gokul Raja[1],
Silambuselvan Parani Bramma Nayagi[1] and Karthikeyan Krishnamoorthy[2*]

1 Department of Mechanical Engineering, Centre for Nano Science and Technology, Mepco Schlenk Engineering College, Sivakasi, India

2 Nanomaterials and System Laboratory, Major of Mechatronics Engineering, Faculty of Applied Energy System, Jeju National University, Jeju, South Korea

*Address all correspondence to: kjeya@mepcoeng.ac.in
and karthi.nanotech@gmail.com

IntechOpen

References

[1] X. Zhang, F. Shi, J. Niu, Y. Jiang, Z. Wang, Superhydrophobic surfaces: From structural control to functional application, J. Mater. Chem. 18 (2008) 621-633. doi:10.1039/b711226b.

[2] S. S. Latthe, R. S. Sutar, V. S. Kodag, A. K. Bhosale, A. MadhanKumar, K. K. Sadasivuni, R. Xing, S. Liu, Self – cleaning superhydrophobic coatings: Potential industrial applications, Prog. Org. Coat. 128 (2019) 52-28. 10.1016/j.porgcoat.2018.12.008. LECTACTA.2017.01.044.

[3] T. Yang, M. Wang, X. Wang, X. Di, C. Wang, Y. Li, Fabrication of a waterborne, superhydrophobic, self-cleaning, highly transparent and stable surface, Soft Matter 16 (2020) 3678-3685. doi: 10.1039/C9SM02473E.

[4] X. Dong, J. Meng, Y. Hu, X. Wei, X. Luan, H. Zhou, Fabrication of Self-Cleaning Superhydrophobic Surfaces with Improved Corrosion Resistance on 6061 Aluminum Alloys, Micromachines (Basel). 11 (2020) 159. doi: 10.3390/mi11020159.

[5] C. Neinhuis, Characterization and Distribution of Water-repellent, Self-cleaning Plant Surfaces, Ann. Bot. 79 (1997) 667-677. doi:10.1006/anbo.1997.0400.

[6] K. Watanabe, Yanuar, H. Udagawa, Drag reduction of Newtonian fluid in a circular pipe with a highly water-repellent wall, J. Fluid Mech. 381 (1999) 225-238. doi:10.1017/S0022112098003747.

[7] T. Liu, Y. Yin, S. Chen, X. Chang, S. Cheng, Super-hydrophobic surfaces improve corrosion resistance of copper in seawater, Electrochim. Acta. 52 (2007) 3709-3713. doi:10.1016/j.electacta.2006.10.059.

[8] M. Ma, R.M. Hill, J.L. Lowery, S. V. Fridrikh, G.C. Rutledge, Electrospun poly(styrene-block-dimethylsiloxane) block copolymer fibers exhibiting superhydrophobicity, Langmuir. 21 (2005) 5549-5554. doi:10.1021/la047064y.

[9] J. Kadarkaraithangam, M. Anthony Raja, K. Krishnamoorthy, S. Natarajan, Fabrication of superhydrophobic surfaces using CuO nanoneedles blended polymer nanocomposite film, Nanosci. Nanotechnol. Lett. 5 (2013) 558-562. doi:10.1166/nnl.2013.1579.

[10] A. Lafuma, D. Quéré, Superhydrophobic states, Nat. Mater. 2 (2003) 457-460. doi:10.1038/nmat924.

[11] A.B.D. Cassie, S. Baxter, Wettability of porous surfaces, Trans. Faraday Soc. 40 (1944) 546-551. doi:10.1039/tf9444000546.

[12] R.N. Wenzel, Resistance of solid surfaces to wetting by water, Ind. Eng. Chem. 28 (1936) 988-994. doi:10.1021/ie50320a024.

[13] X.M. Li, D. Reinhoudt, M. Crego-Calama, What do we need for a superhydrophobic surface? A review on the recent progress in the preparation of superhydrophobic surfaces, Chem. Soc. Rev. 36 (2007) 1350-1368. doi:10.1039/b602486f.

[14] A. Otten, S. Herminghaus, How Plants Keep Dry: A Physicist's Point of View, Langmuir. 20 (2004) 2405-2408. doi:10.1021/la034961d.

[15] A. Scardino, R. De Nys, O. Ison, W. O'Connor, P. Steinberg, Microtopography and antifouling properties of the shell surface of the bivalve molluscs *Mytilus galloprovincialis* and *Pinctada imbricata*, in: Biofouling, Biofouling, 2003: pp. 221-230. doi:10.1080/0892701021000057882.

[16] K Y. Suh, S. Jon, Control over Wettability of Polyethylene Glycol

Surfaces Using Capillary Lithography, Langmuir 21 (2005) 6836-6841. doi:10.1021/LA050878+.

[17] D. Öner, T.J. McCarthy, Ultrahydrophobic surfaces. Effects of topography length scales on wettability, Langmuir. 16 (2000) 7777-7782. doi:10.1021/la000598o.

[18] J. Fresnais, L. Benyahia, F. Poncin-Epaillard, Dynamic (de)wetting properties of superhydrophobic plasma-treated polyethylene surfaces, Surf. Interface Anal. 38 (2006) 144-149. doi:10.1002/sia.2235.

[19] Y. Wu, M. Bekke, Y. Inoue, H. Sugimura, H. Kitaguchi, C. Liu, O. Takai, Mechanical durability of ultra-water-repellent thin film by microwave plasma-enhanced CVD, in: Thin Solid Films, Elsevier, 2004: pp. 122-127. doi:10.1016/j.tsf.2003.12.007.

[20] J.T. Han, Y. Zheng, J.H. Cho, X. Xu, K. Cho, Stable superhydrophobic organic-inorganic hybrid films by electrostatic self-assembly, J. Phys. Chem. B. 109 (2005) 20773-20778. doi:10.1021/jp052691x.

[21] G. Zhang, D. Wang, Z.Z. Gu, H. Mchwald, Fabrication of superhydrophobic surfaces from binary colloidal assembly, Langmuir. 21 (2005) 9143-9148. doi:10.1021/la0511945.

[22] H. Yabu, M. Shimomura, Single-step fabrication of transparent superhydrophobic porous polymer films, Chem. Mater. 17 (2005) 5231-5234. doi:10.1021/cm051281i.

[23] K. Acatay, E. Simsek, C. Ow-Yang, Y.Z. Menceloglu, Tunable, superhydrophobically stable polymeric surfaces by electrospinning, Angew. Chemie - Int. Ed. 43 (2004) 5210-5213. doi:10.1002/anie.200461092.

[24] A. Kavitha Sri, P. Deeksha, G. Deepika, J. Nishanthini, G.S. Hikku, S. Antinate Shilpa, K. Jeyasubramanian, R. Murugesan, Super-hydrophobicity: Mechanism, fabrication and its application in medical implants to prevent biomaterial associated infections, J. Ind. Eng. Chem. 92 (2020) 1-17. doi:10.1016/j.jiec.2020.08.008.

[25] R. Liao, C. Li, Y. Yuan, Y. Duan, A. Zhuang, Anti-icing performance of ZnO/SiO_2/PTFE sandwich-nanostructure superhydrophobic film on glass prepared via RF magnetron sputtering, Mater. Lett. 206 (2017) 109-112. doi:10.1016/j.matlet.2017.06.127.

[26] Z. Li, B.L. Nguyen, Y.C. Cheng, J. Xue, G. MacLaren, C.H. Yap, Durable, flexible, superhydrophobic and blood-repelling surfaces for use in medical blood pumps, J. Mater. Chem. B. 6 (2018) 6225-6233. doi:10.1039/C8TB01547C.

[27] Y. Wu, J. Wen, P. Zhang, Application of AOI light source modes in multi-chip modules inspection, in: Proc. - 2018 19th Int. Conf. Electron. Packag. Technol. ICEPT 2018, Institute of Electrical and Electronics Engineers Inc., 2018: pp. 141-143. doi:10.1109/ICEPT.2018.8480769.

[28] V.A. Lifton, S. Simon, R.E. Frahm, Reserve battery architecture based on superhydrophobic nanostructured surfaces, Bell Labs Tech. J. 10 (2005) 81-85. doi:10.1002/bltj.20105.

[29] Y. Si, Z. Guo, Superhydrophobic nanocoatings: From materials to fabrications and to applications, Nanoscale. 7 (2015) 5922-5946. doi:10.1039/c4nr07554d.

[30] M. Shateri Khalil-Abad, M.E. Yazdanshenas, Superhydrophobic antibacterial cotton textiles, J. Colloid Interface Sci. 351 (2010) 293-298. doi:10.1016/j.jcis.2010.07.049.

[31] K. Jeyasubramanian, G.S. Hikku, A.V.M. Preethi, V.S. Benitha, N.

Selvakumar, Fabrication of water repellent cotton fabric by coating nano particle impregnated hydrophobic additives and its characterization, J. Ind. Eng. Chem. 37 (2016) 180-189. doi:10.1016/j.jiec.2016.03.023.

[32] G.R.T. Suyambulingam, K. Jeyasubramanian, V.K. Mariappan, P. Veluswamy, H. Ikeda, K. Krishnamoorthy, Excellent floating and load bearing properties of superhydrophobic ZnO/copper stearate nanocoating, Chem. Eng. J. 320 (2017). doi:10.1016/j.cej.2017.03.052.

[33] T.S.G. Raja, K. Jeyasubramanian, Tuning the superhydrophobicity of magnesium stearate decorated ZnO porous structures for self-cleaning urinary coatings, Appl. Surf. Sci. 423 (2017) 293-304. doi:10.1016/j.apsusc.2017.06.188.

[34] H.E. Yong, K. Krishnamoorthy, K.T. Hyun, S.J. Kim, Preparation of ZnO nanopaint for marine antifouling applications, J. Ind. Eng. Chem. 29 (2015) 39-42. doi:10.1016/j.jiec.2015.04.020.

[35] S. Thangavel, K. Krishnamoorthy, V. Krishnaswamy, N. Raju, S.J. Kim, G. Venugopal, Graphdiyne-ZnO Nanohybrids as an Advanced Photocatalytic Material, J. Phys. Chem. C. 119 (2015) 22057-22065. doi:10.1021/acs.jpcc.5b06138.

[36] A.U. Dogan, M. Dogan, M. Omal, Y. Sarikaya, A. Aburub, D.E. Wurster, Baseline studies of The Clay Minerals Society source clays: Specific surface area by Brunauer Emmett Teller (BET) method, Clays Clay Miner. 54 (2006) 62-66. doi:10.1346/CCMN.2006.0540108.

[37] J. Li, X. Liu, Y. Ye, H. Zhou, J. Chen, A facile solution-immersion process for the fabrication of superhydrophobic surfaces with high water adhesion, Mater. Lett. 66 (2012) 321-323. doi:10.1016/j.matlet.2011.08.044.

[38] Y. Huang, D.K. Sarkar, X.G. Chen, A one-step process to engineer superhydrophobic copper surfaces, Mater. Lett. 64 (2010) 2722-2724. doi:10.1016/j.matlet.2010.09.010.

[39] N. Xu, D.K. Sarkar, X. Grant Chen, H. Zhang, W. Tong, Superhydrophobic copper stearate/copper oxide thin films by a simple one-step electrochemical process and their corrosion resistance properties, RSC Adv. 6 (2016) 35466-35478. doi:10.1039/c6ra01944g.

[40] Y. Zhang, P. Ju, C. Zhao, X. Qian, In-situ Grown of MoS2/RGO/MoS2@Mo Nanocomposite and Its supercapacitor Performance, Electrochim. Acta. 219 (2016) 693-700. doi:10.1016/j.electacta.2016.10.072.

[41] C.A. Schneider, W.S. Rasband, K.W. Eliceiri, NIH Image to ImageJ: 25 years of image analysis, Nat. Methods. 9 (2012) 671-675. doi:10.1038/nmeth.2089.

[42] S.A. Mahadik, F. Pedraza, R.S. Vhatkar, Silica based superhydrophobic coating for long-term industrial and domestic applications, J. Alloys Compd. 663 (2016) 487-493. doi:10.1016/j.jallcom.2015.12.016.

[43] B. V. Ramana, A. Das, S. Dhara, S. Amirthapandian, A.K. Tyagi, Synthesis and surface functionalization of SnO2 nanoparticles and their superhydrophobic coatings, Sci. Adv. Mater. 5 (2013) 865-872. doi:10.1166/sam.2013.1532.

[44] X.Q. Kong, J.L. Liu, W.J. Zhang, Y.D. Qu, Load-bearing ability of the mosquito tarsus on water surfaces arising from its flexibility, AIP Adv. 5 (2015) 037101. doi:10.1063/1.4908027.

[45] Q. Pan, M. Wang, Miniature boats with striking loading capacity fabricated

from superhydrophobic copper meshes, ACS Appl. Mater. Interfaces. 1 (2009) 420-423. doi:10.1021/am800116d.

[46] X. Zhang, J. Zhao, Q. Zhu, N. Chen, M. Zhang, Q. Pan, Bioinspired aquatic microrobot capable of walking on water surface like a water strider, ACS Appl. Mater. Interfaces. 3 (2011) 2630-2636. doi:10.1021/am200382g.

[47] J.L. Liu, X.Q. Feng, G.F. Wang, Buoyant force and sinking conditions of a hydrophobic thin rod floating on water, Phys. Rev. E - Stat. Nonlinear, Soft Matter Phys. 76 (2007) 066103. doi:10.1103/PhysRevE.76.066103.

[48] G. He, S. Lu, W. Xu, S. Szunerits, R. Boukherroub, H. Zhang, Controllable growth of durable superhydrophobic coatings on a copper substrate via electrodeposition, Phys. Chem. Chem. Phys. 17 (2015) 10871-10880. doi:10.1039/c5cp00059a.

[49] Self-cleaning flow shut off valve, 2010.

[50] Toilet bowl cleaning and/or deodorizing device, 2011. www.dripirrigation.com, (accessed November 7, 2020).

[51] N.B. Vargaftik, B.N. Volkov, L.D. Voljak, International Tables of the Surface Tension of Water, J. Phys. Chem. Ref. Data. 12 (1983) 817-820. doi:10.1063/1.555688.

[52] C.O. Mills, E. Ellas, G.H.B. Martin, M.T.C. Woo, A.F. Winder, Surface Tension Properties of Human Urine: Relationship with Bile Salt Concentration1), Clin. Chem. Lab. Med. 26 (1988) 187-194. doi:10.1515/cclm.1988.26.4.187.